INDIAN JOURNAL OF SCIENCE AND TECHNOLOGY

RESEARCH ARTICLE

Metal Cored Wire on Mechanical Properties and Microstructural Characteristics of Wire Arc Direct Energy Deposited Component

B Prabhakaran[1]*, P Sivaraj[1], S Malarvizhi[1], V Balasubramanian[1], S Sathiya[2]

1 Centre for Materials Joining and Research (CEMAJOR), Department of Manufacturing Engineering, Annamalai University, Annamalai Nagar, Chidambaram, 608002, Tamil Nadu, India
2 Department of Computer Science and Engineering, Annamalai University, Annamalai Nagar, Chidambaram, 608002, Tamil Nadu, India

OPEN ACCESS

Received: 25-10-2024
Accepted: 20-11-2024
Published: 05-12-2024

Citation: Prabhakaran B, Sivaraj P, Malarvizhi S, Balasubramanian V, Sathiya S (2024) Metal Cored Wire on Mechanical Properties and Microstructural Characteristics of Wire Arc Direct Energy Deposited Component. Indian Journal of Science and Technology 17(44): 4655-4662. https://doi.org/10.17485/IJST/v17i44.3514

* **Corresponding author**.

rsamuniv2021@gmail.com

Funding: None

Competing Interests: None

Published By Indian Society for Education and Environment (iSee)

ISSN
Print: 0974-6846
Electronic: 0974-5645

Abstract

Objectives: Fabrication of a cylinder-shaped High-Strength Low Alloyed steel wall component through wire (metal cored) arc additive manufacturing and assess the homogeneity and integrity of the built component. **Method**: Mechanical testing and microstructural characterizations such as optical microscopy, scanning electron microscopy and electron backscattered diffraction techniques were performed at distinct regions (namely, bottom and top). **Findings**: The conducted tensile test at the bottom area recorded a tensile strength of 864 MPa, which is 5.9 % higher than the top region but with a lower total elongation. The microhardness study revealed that the average hardness at the bottom region was 266 $HV_{0.5}$, while the top region was 241 $HV_{0.5}$. The microstructural analysis conducted in both areas indicates that the bottom region exhibits better hardness and strength due to the presence of a high value of geometrically necessary dislocations, High-Angle Grain Boundaries and increased grains with reduced size. However, the built component proves to have better homogeneity with marginal deviations in the properties estimated. **Novelty**: Solid wire was used as a predominant filler material for the Wire-Arc Additive Manufacturing (WAAM) process, which requires high heat input to melt the material. Hence, to reduce the heat input, metal-cored wire was used instead of solid wire for the Gas Metal Arc -WAAM process.

Keywords: Gas metal arc welding; Metal cored wire; Mechanical properties; Direct energy deposition; Wire-arc additive manufacturing

1 Introduction

The High-Strength Low Alloy (HSLA) steels are broadly employed in marine, construction, tool, and die industries and, more specifically, bridges, ship plates, and offshore platforms to manufacture large-sized structural components due to their excellent weldability. Added to the weldability, the alloy also exhibits balanced

mechanical properties due to its chemical composition wherein the carbon content is kept low with the range of 0.25 wt. % and total weight percentage of elements like Mo, Cr, Mn, Nb, Ni, and Ti below 2.5 wt. %. Owing to this, HSLA steel features low cost and good processability and reserves its position in various industrial applications [1,2]. Conventional casting technology is commonly used to develop large-sized HSLA steel components. A recent study also found that Wire-Arc Additive Manufacturing (WAAM) exhibits better strength and microstructural properties than the casting technique. Zhang et al. [3] investigated the effect of WAAM and Casting techniques on the fabrication of HSLA parts. The study confirmed that the WAAM component exhibited a 10.31 % increase in ultimate tensile strength and an 89.9 % increase in elongation than the casted component.

Generally, arc energy is used as a heat source for the WAAM technique. However, Zhang et al. [4] reported using the Wire-fed Laser Additive Manufacturing (LAM-W) technique for the fabrication of components and correlated the results with the conventional WAAM process. They confirmed that LAM-W has excellent weld pool stability. Yet, the deposition rate of the WAAM was 1.5 times better than the LAM-W. Such findings have widely exploited the use of WAAM in fabricating HSLA steel of large-sized and complex shape components [5,6]. Based on the inferences, this study used WAAM techniques to fabricate HSLA components. Yet, during the fabrication of components, depending on the shape and height, the number of layers required to deposit may vary even for the optimized processing condition. It was also inferred that each layer was influenced by different thermal cycles during deposition [6–8], thus influencing microstructure and local mechanical properties at various heights. Hence, to control thermal cycles, heat input must be given significant concern, as it causes grain coarsening during solidification. This decreases the hardness and strength of the components. Fang et al. [9] suggested that the low heat input during the process could significantly control grain growth, avoid material softening, and enhance material strength**.** Hence, reducing heat input during the WAAM process is paramount.

Furthermore, studies have been mainly carried out using solid wire electrodes as filler wire for the WAAM process [10,11]. The potential drawback of using solid wire is that the current required to melt the wire depends on the cross-section of the wire. The cases that require a higher deposition rate require a higher current to melt the solid wire. This increase in current increases the heat input and significantly affects the metallurgical and mechanical properties of the component. Hence, without sacrificing the deposition rate, the heat input of the deposition needs to be reduced. The metal-cored wire was used in this study to address this. Thus, Yi et al. [12] explained that using metal-cored wire amalgamates the benefits of both wire and powder. The metal cored wire carries the current in the hollow sheath, which increases the current density at low amperage, thus reducing the heat input of the deposition without affecting the deposition rate [13,14]. From the literature, it is also evident that a limited number of works only focused on developing WAAM components using metal-cored wire. Hence, the research focused extensively on the deposition of metal-cored wire to fabricate the WAAM component using the Gas-Metal Arc Welding (GMAW) technique. This study also assesses the evolution of microstructural and mechanical properties of deposited components in the built direction.

2 Methodology

A cylinder-shaped wall with a dimension of 160 mm height, 52.5 mm radius from the center of the cylinder to the neutral axis of deposition, and wall thickness of 7 mm was fabricated using the Gas-Metal Arc (GMA)- WAAM. The fabricated component, deposition strategy, and scheme of specimen extraction are shown in Figure 1. The filler wire was E110C-K-H4 metal-cored wire with 1.2 mm diameter, and the wire chemistry is presented in Table 1. The parameters used for component fabrication are represented in Table 2.

Table 1. Wire chemistry of metal cored wire (E110C-K-H4)

Elements	C	Si	Mn	P	S	Cr	Ni	Mo	Cu	Fe
Composition (wt. %)	0.06	0.57	1.57	0.009	0.009	0.39	2.24	0.39	0.12	Bal

According to the literature's outcome [1,3,8,15], sample extraction was carried out at the top and bottom of the components, as it became two extremities (high and low) for the mechanical properties. Hence, the top and bottom areas were considered for mechanical and metallurgical evaluations. Tensile specimens were extracted from the deposits according to ASTM E8M and milled to 4 mm for flat geometry. The samples used for the metallographic and microhardness studies were extracted in both regions, as depicted in Figure 1c. Metallographic studies such as Optical Microscopy (OM), Electron Backscattered Diffraction (EBSD) and Scanning Electron Microscopy (SEM) were done for the extracted samples. SEM and OM samples were polished with different grades of emeries and etched with 2 % nital solution, while EBSD samples were just electropolished before the examination. An Instron tensile testing facility was utilized to conduct the tensile test, and the cross-head speed was set to 1 mm/min. An indentation load of 0.5 kg was used during the Vickers microhardness survey, and a dwell time of 15 seconds was maintained. The successive indentation along the build direction was maintained at 1 mm.

Table 2. Process parameters used for fabrication

Current (A)	120
Voltage (V)	14.3
Substrate rotation (rad/min)	5.71
Gas Mixture	Ar: 80 % + CO_2: 20 %
Gas flow rate (litres/minute)	15
Contact tip to workpiece distance (mm)	15
Heat input (kJ/mm)	0.272

3 Results and Discussion

3.1 Microstructural Characterization

Figures 2, 3 and 4 represents the OM, SEM, and EBSD characterizations carried out for the different regions of the built component. Significant characteristic changes were observed in the samples of both regions. The bottom area sample exhibits a coarse columnar structure, while at the top, no discernable columnar grains were observed, as can be witnessed in Figure 2**a** and **c**. There is good agreement between the results of the literature [3,7] and the evolution of columnar morphology in this study. The columnar evolution was due to the induced directional solidification; the prior austenite grains grew in the direction of the highest thermal gradient. This gradient may be initiated by the dissipation of heat from the cold substrate to the depositing layer or between the solidified and relatively cooled previous layer. The morphologies of both samples show the presence of Acicular Ferrite (AF), Granular Bainite (GB), and Quasi-Polygonal Ferrite (QPF) in Figure 2**b** & **d** while SEM analysis (Figure 2 **e** & **f**) reveals the lath Martensite/Bainitic Ferrite (ML/BF) and Tempered Bainite (TB) [16]. The subsequent deposition of layers causes the formation of tempered bainite because the thermal cycles related to each deposition cause a tempering effect [1]. Yet, the sizes of the tempered bainite were different. The top region consists of a wider width and shorter length of bainite, while the opposite was observed in the bottom area with finer bainite. This observation relates to the dominant heat dissipation mechanism in the top region through the surrounding medium by radiation because previously deposited layers possess more accumulated heat [3]. Furthermore, Xu et al. [7] reported that the top region had a higher peak temperature than the bottom region, and the cooling rate within the bottom area was higher due to the heat-dissipating abilities of the earlier deposited layers. The lath martensite/bainitic ferrite formed at the bottom region is also associated with a faster cooling rate.

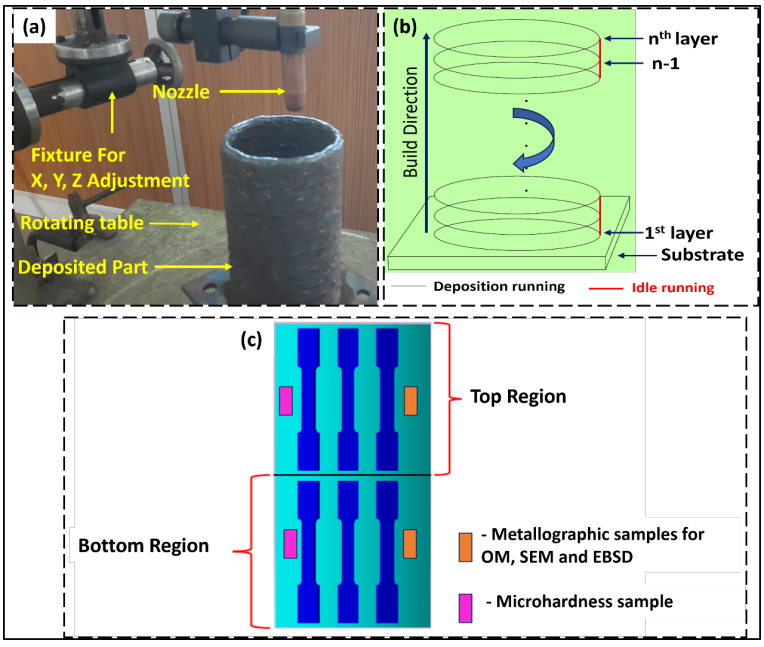

Fig 1. (a) Deposited WAAM component; (b) deposition of strategy; (c) scheme of specimen extraction

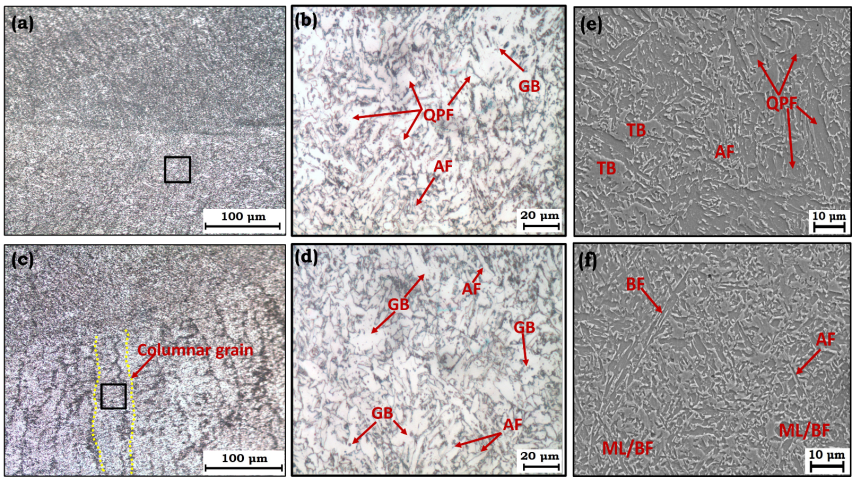

Fig 2. Microstructure of Build sample: (a-d) OM images; (e, f) SEM image; (a, b, e) Top region; (c, d, f) Bottom region

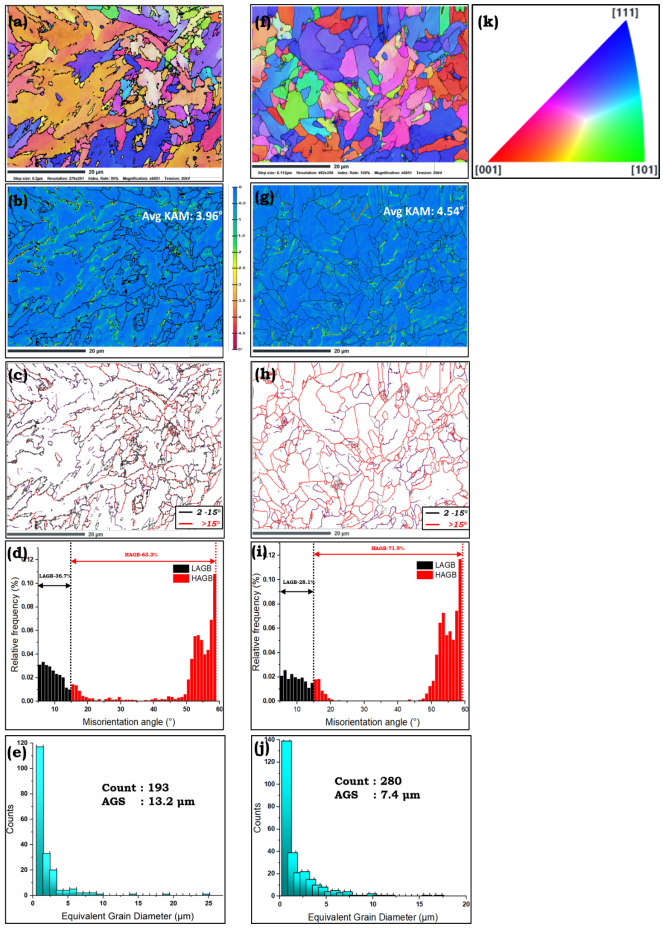

Fig 3. EBSD Plot of (a-e) Top and (f-j) Bottom region: (a, f) Inverse pole figure; (b, g) Kernel average misorientation map; (c, h) LAGB and HAGB distribution; (d, i) LAGB and HAGB plot; (e, j) Grain size distribution ; (k) Inverse pole figure triangle with direction

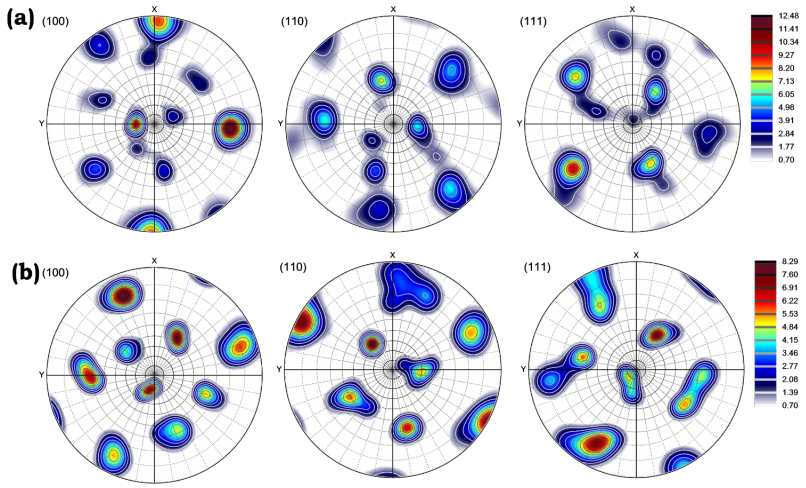

Fig 4. Pole figure image of (a) Top and (b) Bottom region

The inverse pole figure from the EBSD plot shown in Figure 3**a** and **f** reveals the coarser grain in the top region while the finer grain is at the bottom. Further, an average grain size of 7.4 μm among 280 scanned grains was observed in the bottom area, and the differences in the grain size and counts are depicted in Figure 3 **e** and **j**. These results agree with the earlier discussion of fine ferrite morphology in the bottom region. It was evident from the inverse pole figure of the top area that most of the grains, especially the coarser grains, have similar colors (i.e., grains are oriented in specific directions). Figure 4 shows a relatively higher texture index (12.48 mud) in the top region than in the bottom (8.29 mud), representing the grains in the top area being oriented in a specific direction. According to Xu et al.[17], the heat accumulation due to cyclic heating generates enough activation for the atoms to find a place in the existing crystal, thus limiting the atoms to create nucleation. Hence, this results in the coarsening of grains in the preferred direction. Following the earlier discussion, the top part exhibits similar conditions with more accumulated heat.

On the other hand, the cooling rate is faster at the bottom region, which favorably weakens the texture by nucleating new crystals/grains in random orientation and restricting grain growth. This phenomenon is attributable to the increased grain count and decrease in size at the bottom region. The misorientation angle analysis shown in Figure 3**c** & **h** reveals that the samples are predominant with angles higher than 15 °, indicating High-Angle Grain Boundaries (HAGBs) formation. The HAGBs contribute significantly to inhibiting the propagation of cracks[18]. Yet, there is a higher proportion at the bottom of the region, which is also true for Low-Angle Grain Boundaries (LAGBs).

3.2 Microhardness variation

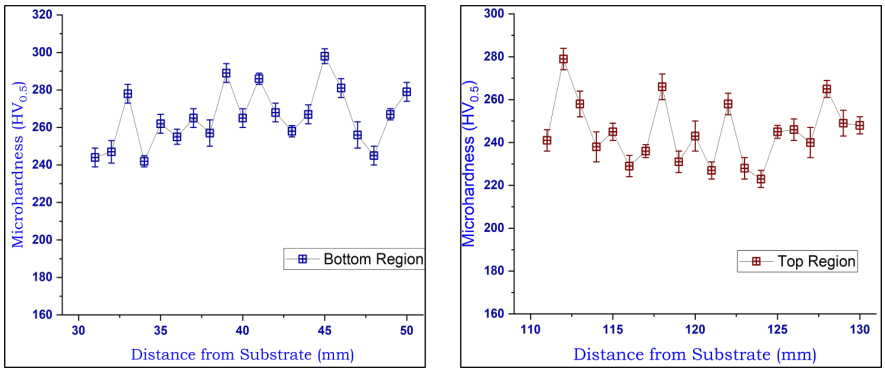

Fig 5. Microhardness distribution of top and bottom region

Figure 5 depicts the variation in microhardness and its distribution in both regions. The average hardness of the top region was 241 $\pm$ 14.8 $HV_{0.5}$, while the bottom region exhibited 266 $\pm$ 15.6 $HV_{0.5}$, respectively. The bottom region shows a marginal rise in hardness due to the refined grains of hard phases such as martensite and bainite. Grain coarsening was caused by the accumulation of thermal energy along the build direction [8] and the slower rate of cooling at the top region resulted in decreased hardness [7]. The absence of hard phases in the top region could be ascribed to coarser grains, thus acting as a mechanical barrier to have martensite transformation [16]. Finer grains play a predominant role in increasing hardness and are defined by the Hall-Petch equation [18,19]. Accordingly, the variation in average microhardness between the top and bottom areas of the component was 9 %, indicating that the component was homogeneous throughout its structure.

3.3 Tensile Properties

The scheme of specimens' extraction was illustrated in the schematic Figure 1**c**. The stress vs strain curve was plotted and shown in Figure 6. The as-deposited build's yield strength (σ_y) and ultimate tensile strength (σ_u) decreased from 657 MPa to 644 MPa and 864 MPa to 816 MPa along the build direction, respectively. Whilst the total elongation (ε_{total}) increased from 21.6 % to 23.2 %. A similar trend was reported by Zhang et al. [3]. The increased strength was related to geometrical necessary dislocation, grain size refinement, and high-angle grain boundary formation. The Kernel Average Misorientation (KAM) value is directly proportional to the geometrically necessary dislocations, which are required to cause a slip in the system [20]. The increase in KAM value represents increased dislocation density formed in the structure. The system's yield strength increases with increased dislocation density [9]. Secondly, the finer grain size will increase the stress required to cause a dislocation slip and act as a pinning point for the dislocation movement, thus increasing the strength of the bottom region [1]. Lastly, highly strained grains oriented in a random direction cause the formation of HAGBs, and these HAGBs hinder crack propagation by inhibiting the movement of dislocations through dislocation entanglements. The results plotted in Figure 3**b, d, e** and Figure 3 **g, i, j** depicts that the KAM value, HAGBs proportion, and grain size are higher in the bottom area when comparing the top and well in agreement with the increase in strength at the bottom area. Compared to the casted component from the literature [21], the average $\sigma_{u,}$ and σ_y of the WAAM component was increased from 728 MPa to 840 MPa, and 565 MPa to 651 MPa respectively. This signifies that the component fabricated through WAAM techniques was better than the casted component.

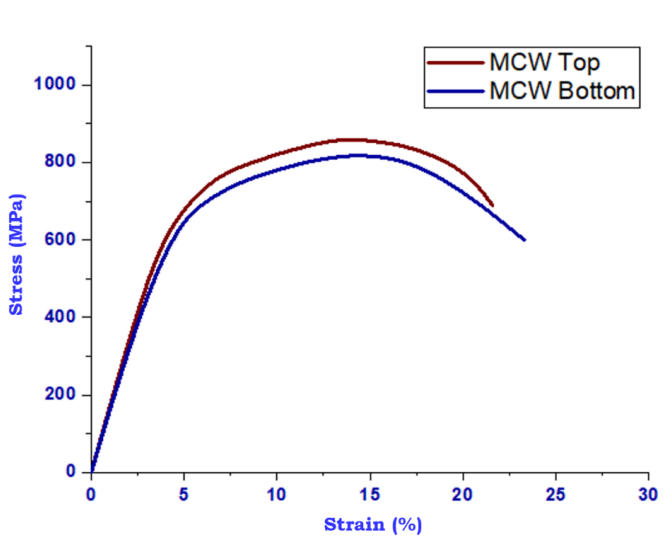

Fig 6. Stress vs strain plot

From Table 3, it is obvious that the study proved that metal-cored wire has 6.5 % higher σ_u than the component manufactured through solid wire (ER110S-G) using Cold Metal Transfer (CMT)-WAAM process. CMT, by mechanism, produces less heat input than the GMAW [22]. The present study, which used metal-cored wire, reduced the heat input of the process and brought it closer to CMT [23]. Added to this, the heat input of the present study is 46.38 % less than the heat input reported by Rodrigues et al. [8], wherein their work utilized the same GMA-WAAM to deposit the solid wire of similar composition as presented in Table 1. Consequently, 11. 3 % higher σ_u and 16. 60 % higher ε_{total} is attained in the present study compared to the literature work [8]. Thus, it justifies the novelty of the work.

Table 3. Comparison of the present study with Cold Metal Transfer (CMT) and GMAW-WAAM

Process	Filler wire	Heat input (kJ/mm)	Average σ_u (MPa)	Average ε_{total} (%)	References
CMT-WAAM	ER110S-G	0.272	788 ± 10	19.05 ± 0.2	[23]
GMA-WAAM	ER110S-G	0.511	755 ± 12	19.21 ± 0.5	[8]
GMA-WAAM	E110C-K-H4	0.274	840 ± 24	22.40 ± 0.8	Present study

The SEM fractography in Figure 7 of both regions reveals dimples, tear ridges, and micro-voids, indicating the failure mode is a ductile fracture[24]. Yet, the dimples in the bottom region are equiaxed, indicating a homogenous stress distribution along the fractured surface under tensile loading. The homogeneous distribution of dimples infers that the fracture initiation was governed by the nucleation of micro-voids whereas the dimples in the top region exhibited uneven distribution of stress. Further, the larger and deeper dimples enable better ductility in the top area[19] whereas dimples in the bottom region are higher and could be ascribed to increased strength.

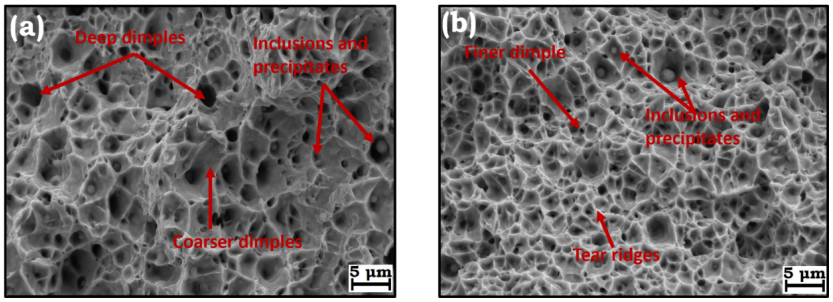

Fig 7. Fractographyof (a) top and (b) bottom region

4 Conclusion

The study explored the variation of mechanical properties and microstructural morphologies at different regions of components built with metal-cored wire using the GMA-WAAM technique. It also analyzed the influence of process and filler wire chemistry on the deposited WAAM component. It proved that the component fabricated using metal-cored wire exhibits better properties than the conventional casting technique and the cold metal transfer WAAM technique. The metal-cored wire also exhibited 46.38 % less heat input than the solid wire. Hence, the study recommends using metal-cored wire instead of solid wire and the WAAM technique instead of conventional casting to fabricate HSLA components. The other significant findings are below.

- The aesthetic of fabricated components proves that the build is free from significant defects.
- The strength and microhardness properties of the top region were inferior to those of the bottom region, yet the total elongation was marginally higher in the top region.
- The coarser grain, low dislocation density value, and low number of HAGBs at the top region caused an increase of about 7.4 % of total elongation and decreased strength and hardness.
- Grain coarsening was the prime cause of decreased mechanical properties in the top region.
- The bottom area of the specimen exhibited finer grain, hard phases of martensite/bainite morphology, and an acicular ferrite structure.
- The finer grains and high percentage of HAGBs cause a hindrance to dislocation movement, thereby increasing the strength of the bottom region.

References

1) Rodrigues TA, Duarte VR, Tomás D, Avila JA, Escobar JD, Rossinyol E, et al. In-situ strengthening of a high strength low alloy steel during Wire and Arc Additive Manufacturing (WAAM). *Additive Manufacturing*. 2020;34. Available from: https://doi.org/10.1016/j.addma.2020.101200.
2) Tian Y, Zhou J, Shen Y, Qu Z, Xue W, Wang Z. Improved Toughness of a High-Strength Low-Alloy Steel for Arctic Ship by Ni and Mo Addition. *Advanced Engineering Materials*. 2020;22(6). Available from: https://doi.org/10.1002/adem.201901553.

3) Zhang W, Shang X, Chen S, Zhang L. Comparison of microstructural characteristics and mechanical properties of the high-strength low-alloy steels fabricated by wire arc additive manufacturing versus conventional casting. *Materials Science and Engineering: A*. 2023;885(3). Available from: https://doi.org/10.1016/j.msea.2023.145593.
4) Zhang D, Fang Q, Li B, Wang Y, Si S, Jiang Y. A Comparative Study of Microstructural Characteristics and Mechanical Properties of High-Strength Low-Alloy Steel Fabricated by Wire-Fed Laser Versus Wire Arc Additive Manufacturing. *Crystals*. 2024;14(6). Available from: https://doi.org/10.3390/cryst14060528.
5) Marques DA, Oliveira JP, Baptista AC. A Short Review on the Corrosion Behaviour of Wire and Arc Additive Manufactured Materials. *Metals*. 2023;13(4):1–19. Available from: https://doi.org/10.3390/met13040641.
6) li Dai Y, fu Yu S, guo Huang A, sheng Shi Y. Microstructure and mechanical properties of high-strength low alloy steel by wire and arc additive manufacturing. *International Journal of Minerals, Metallurgy and Materials*. 2020;27(7):933–942. Available from: https://link.springer.com/article/10.1007/s12613-019-1919-1.
7) Xu M, Chen S, Yuan T, Jiang X, Zhang H. Effect of thermal cycles on the microstructure and properties of the Al-Zn-Mg-Cu alloy during wire-arc additive manufacturing. *Journal of Alloys and Compounds*. 2022;928. Available from: https://doi.org/10.1016/j.jallcom.2022.167172.
8) Rodrigues TA, Duarte V, Avila JA, Santos TG, Miranda RM, Oliveira JP. Wire and arc additive manufacturing of HSLA steel: Effect of thermal cycles on microstructure and mechanical properties. *Additive Manufacturing*. 2019;27:440–450. Available from: https://doi.org/10.1016/j.addma.2019.03.029.
9) Fang Q, Zhao L, Chen C, Zhu Y, Peng Y, Yin F. Effect of heat input on microstructural and mechanical properties of high strength low alloy steel block parts fabricated by wire arc additive manufacturing. *Materials Today Communications*. 2023;34. Available from: https://doi.org/10.1016/j.mtcomm.2022.105146.
10) Su C, Chen X, Gao C, Wang Y. Effect of heat input on microstructure and mechanical properties of Al-Mg alloys fabricated by WAAM. *Applied Surface Science*. 2019;486:431–440. Available from: https://doi.org/10.1016/j.apsusc.2019.04.255.
11) Le VT, Mai DS, Doan TK, Paris H. Wire and arc additive manufacturing of 308L stainless steel components: Optimization of processing parameters and material properties. *Engineering Science and Technology, an International Journal*. 2021;24(4):1015–1026. Available from: https://doi.org/10.1016/j.jestch.2021.01.009.
12) Yi H, Jia L, Ding J, Li H. Achieving material diversity in wire arc additive manufacturing: Leaping from alloys to composites via wire innovation. *International Journal of Machine Tools and Manufacture*. 2024;194:1–53. Available from: https://doi.org/10.1016/j.ijmachtools.2023.104103.
13) Lin Z, Goulas C, Ya W, Hermans MJM. Microstructure and Mechanical Properties of Medium Carbon Steel Deposits Obtained via Wire and Arc Additive Manufacturing Using Metal-Cored Wire. *Metals*. 2019;9(6). Available from: https://doi.org/10.3390/met9060673.
14) Zhai W, Wu N, Zhou W. Effect of Interpass Temperature on Wire Arc Additive Manufacturing Using High-Strength Metal-Cored Wire. *Metals*. 2022;12(2):1–15. Available from: https://doi.org/10.3390/met12020212.
15) Dash A, Squires L, Avila JD, Bose S, Bandyopadhyay A. Influence of active cooling on microstructure and mechanical properties of wire arc additively manufactured mild steel. *Frontiers in Mechanical Engineering*. 2023;9. Available from: https://doi.org/10.3389/fmech.2023.1130407.
16) Dirisu P, Ganguly S, Mehmanparast A, Martina F, Williams S. Analysis of fracture toughness properties of wire + arc additive manufactured high strength low alloy structural steel components. *Materials Science and Engineering: A*. 2019;765. Available from: https://doi.org/10.1016/j.msea.2019.138285.
17) Xu X, Ganguly S, Ding J, Dirisu P, Martina F, Liu X, et al. Improving mechanical properties of wire plus arc additively manufactured maraging steel through plastic deformation enhanced aging response. *Materials Science and Engineering: A*. 2019;747:111–118. Available from: https://doi.org/10.1016/j.msea.2018.12.114.
18) Panicker CTJ, Senthilkumar V. Effect of arc rotation on the enhancement of mechanical properties of ER70S6 in WAAM. *Vacuum*. 2024;220. Available from: https://doi.org/10.1016/j.vacuum.2023.112837.
19) Van Thao Le, Bui MC, Nguyen TD, Van Anh Nguyen, Van Canh Nguyen. On the connection of the heat input to the forming quality in wire-and-arc additive manufacturing of stainless steels. *Vacuum*. 2023;209. Available from: https://dx.doi.org/10.1016/j.vacuum.2023.111807.
20) Zribi Z, Ktari HH, Herbst F, Optasanu V, Njah N. EBSD, XRD and SRS characterization of a casting Al-7wt%Si alloy processed by equal channel angular extrusion: Dislocation density evaluation. *Materials Characterization*. 2019;153:190–198. Available from: https://doi.org/10.1016/j.matchar.2019.04.044.
21) Shi L, Luo K, Wang J, Feng D, Zhang H, Cao X. Failure analysis of an offshore drilling casing under harsh working conditions. *Engineering Failure Analysis*. 2021;120:1–17. Available from: https://doi.org/10.1016/j.engfailanal.2020.105018.
22) Nagasai BP, Malarvizhi S, Balasubramanian V. Effect of welding processes on mechanical and metallurgical characteristics of carbon steel cylindrical components made by wire arc additive manufacturing (WAAM) technique. *CIRP Journal of Manufacturing Science and Technology*. 2022;36:100–116. Available from: https://dx.doi.org/10.1016/j.cirpj.2021.11.005.
23) Prabhakaran B, Sivaraj P, Malarvizhi S, Balasubramanian V. Mechanical and Metallurgical Characteristics of Wire-Arc Additive Manufactured HSLA Steel Component Using Cold Metal Transfer Technique. *Additive Manufacturing Frontiers*. 2024;3(4). Available from: https://doi.org/10.1016/j.amf.2024.200169.
24) Sankar N, Malarvizhi S, Balasubramanian V. Effect of Rotating Arc on Mechanical Properties and Microstructural Characteristics of Gas Metal Arc Welded Carbon Steel Joints. *Metallography, Microstructure, and Analysis*. 2021;10(4):541–559. Available from: https://dx.doi.org/10.1007/s13632-021-00769-z.